

On the Completeness of Atomic Structure Representations

Sergey N. Pozdnyakov,^{1,*} Michael J. Willatt,^{1,*} Albert P. Bartók,²
Christoph Ortner,^{3,†} Gábor Csányi,^{4,‡} and Michele Ceriotti^{1,§}

¹*Laboratory of Computational Science and Modelling, Institute of Materials,
Ecole Polytechnique Fédérale de Lausanne, Lausanne 1015, Switzerland*

²*Department of Physics and Warwick Centre for Predictive Modelling,
School of Engineering, University of Warwick, Coventry CV4 7AL, United Kingdom*

³*Mathematics Institute, University of Warwick, Coventry CV4 7AL, United Kingdom*

⁴*Engineering Laboratory, University of Cambridge,
Trumpington Street, Cambridge CB2 1PZ, United Kingdom*

(Dated: July 21, 2022)

Many-body descriptors are widely used to represent atomic environments in the construction of machine learned interatomic potentials and more broadly for fitting, classification and embedding tasks on atomic structures. It was generally believed that 3-body descriptors uniquely specify the environment of an atom, up to a rotation and permutation of like atoms. We produce several counterexamples to this belief, with the consequence that any interatomic potential, classifier or embedding that uses 3 (or 4)-body features will incorrectly give identical results for different configurations. We discuss factors that mitigate the impact of this fundamental deficiency of invariant features in applications, and explain the success of current “machine-learning” force fields.

Over the past decade tremendous progress has been made in the use of statistical regression to sidestep computationally demanding electronic structure calculations, and obtain “machine-learning” models of materials and molecules, that use as inputs only the chemical nature and coordinates of the atoms[1–10]. A crucial driver of this progress has been the introduction of *representations* of atomic structures: A property associated with the i -th atom can be written as $F_i = \mathcal{F}(\mathcal{X}_i)$, where $\mathcal{X}_i = \{\mathbf{r}_{ij}\}_{j \neq i}$ describes the neighbour environment of the i -th atom. To preserve symmetries of the target property, the representation of \mathcal{X}_i should be equivariant (often simply invariant) with respect to translations, rotations, labelling of identical atoms [11, 12], and often also reflections. Most of the invariant representations [1, 3, 13–15] can be seen as projections onto different bases of many-body correlation functions[16–18]. To stress that our results apply equally to all these frameworks, we use the abstract notation $|\mathcal{X}_i^{(\nu)}\rangle$ to indicate the $(\nu + 1)$ -body correlation, which is centered on the i -th atom [16]. For instance, the 2-body correlation $|\mathcal{X}^{(1)}\rangle$ corresponds to the histogram of interatomic distances r_{ij} (equivalent to the radial distribution function or the 2-body symmetry functions, G_2 , of Ref. [1]). The 3-body correlation $|\mathcal{X}^{(2)}\rangle$ is equivalent to the histogram of triangles, represented by the 3-tuples $(r_{ij}, r_{ij'}, \omega_{ijj'})$, where $\omega_{ijj'} = \hat{\mathbf{r}}_{ij} \cdot \hat{\mathbf{r}}_{ij'}$ (and to the power spectrum [3], or to the 3-body symmetry functions, G_3 [1]). A linear regression model based on these features is equivalent to a body-ordered expansion of the target property[7, 17–20]. Given that computing higher-order terms is increasingly costly, the representation is typically truncated at 3 or 4 body correlations.

Employing *non-linear* functions of low-order invariants, e.g. $F_i = \tilde{\mathcal{F}}(|\mathcal{X}_i^{(2)}\rangle)$, incorporates information on higher-order correlations, and there is a general belief in

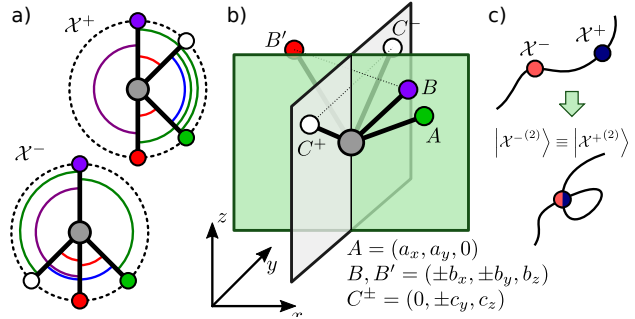


FIG. 1. (a) Two structures with the same histogram of triangles; (angles: $45^\circ, 45^\circ, 90^\circ, 135^\circ, 135^\circ, 180^\circ$) (b) A manifold of degenerate pairs of environments: In addition to three points A, B, B' a fourth point C^+ or C^- is added leading to two degenerate environments, \mathcal{X}^+ and \mathcal{X}^- . (c) Degeneracies induce a transformation of feature space so that structures that should be far apart are brought close together.

the community that, in particular, the 3-body correlation unequivocally identifies an atomic environment. Such injectivity of the structure-representation map would guarantee that any atom-centered property can be described by $\tilde{\mathcal{F}}$, which extends to any atom-centered decomposition of extensive properties, such as the total energy[7]. In this Letter, we present several counterexamples to this widely-held belief, discuss the implications for machine learning atomistic properties, and suggest directions towards the construction of injective representations.

Figure 1a exhibits a simple example of a pair of environments, \mathcal{X}^+ and \mathcal{X}^- , with four neighbouring atoms of the same species positioned on a circle around the central atom. The two structures cannot be superimposed by rotations and mirror symmetry, but they have the same list of distances and angles and hence cannot be

distinguished by their 3-body correlations.

To elucidate this example, and more generally understand the difficulty of reconstructing an atomic environment from a body order representations, consider the Gram matrix $G_{jj'} = \mathbf{r}_{ij} \cdot \mathbf{r}_{ij'}$, which contains sufficient information to reconstruct a configuration up to an arbitrary rotation or reflection. If all the distances r_{ij} , or the chemical identity of the neighbors, are distinct, one can unequivocally assign distances and angles to a specific atom, and reconstruct the Gram matrix from the unordered list $\{(r_{ij}, r_{ij'}, \omega_{ijj'})\}$. If some of the distances are the same, however, it becomes possible to swap some entries of \mathbf{G} , yielding two or more degenerate environments that are different, but have the same 3-body invariants.

As shown in Fig. 1b, one can generalize the construction to obtain a manifold of degenerate environment pairs parameterised by 7 continuous variables. The total dimensionality of the configuration space of 4 neighbours is $4 \times 3 - 3 = 9$. Thus, the degenerate manifold has a dimension of 7 and a codimension of 2. When going from the $+$ to the $-$ structure in the pair, the elements of the Gram matrix between C -type and B -type points are swapped, leading to non-equivalent structures that have the same 3-body description. This construction can be extended by adding further A or C -type points (increasing the codimension of the degenerate manifold by one) or pairs of B -type points (each pair increasing the codimension by three). Other counterexamples can be found, involving triplets of degenerate structures (see SI). Tight bounds on the codimension of degenerate manifolds and on the multiplicity of degenerate structures is a key aspect in understanding the success of incomplete environment descriptors, but is beyond the scope of the present work. However, the example of Fig. 1b is sharp in the sense that (i) for three or fewer neighbours the 3-body correlation suffices to reconstruct the environment and (ii) for four or more neighbours one can construct a manifold of co-dimension 2 which must contain all degenerate environments. These results, which build on those in Ref. [21], are detailed in the SI. It is unclear to us whether the increase of the co-dimension when neighbors are added in the example of Fig. 1b is specific to our construction, or reflects a general result.

Following the procedure in Fig. 1b, one can produce a pair of degenerate tetrahedral environments, that we label \mathcal{X}^+ and \mathcal{X}^- , corresponding to a CH_4 molecule. Figure 2a shows a portion of the two manifolds (blue and red surfaces, parameterised by two variables q and s) built as a principal component projection of the power spectrum space (details given in the SI). Structures within the two surfaces correspond to configurations that are different from each other, but those along the black line (corresponding to $s = 0$) have identical 2- and 3-body invariants, which therefore cannot distinguish \mathcal{X}^+ and \mathcal{X}^- , and the two manifolds intersect each other. As shown in Fig. 2b, however, both atom-centred properties such as

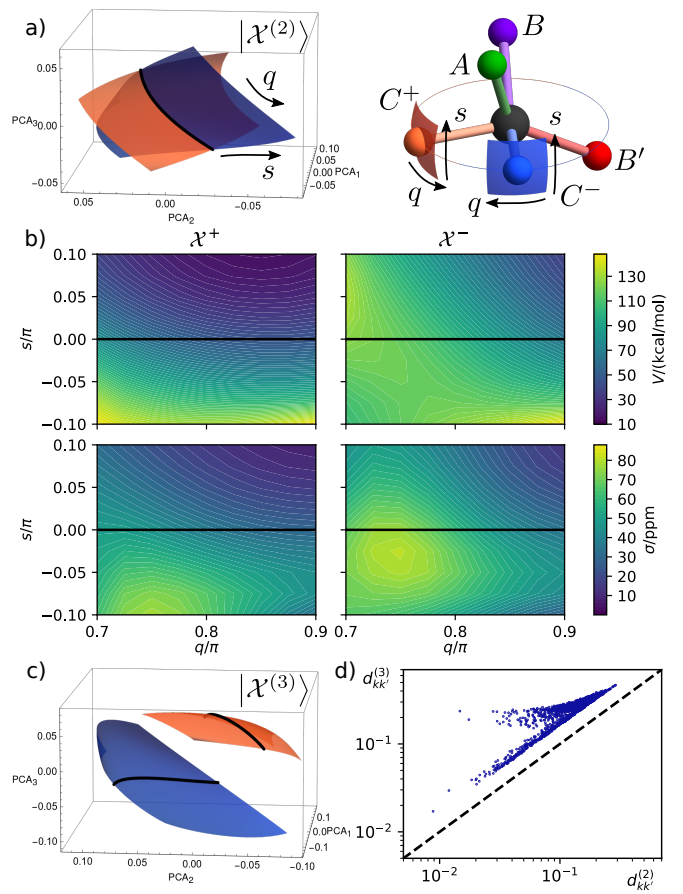


FIG. 2. (a) PCA projection of $|\mathcal{X}^{(2)+}\rangle$ and $|\mathcal{X}^{(2)-}\rangle$ for a continuous manifold of CH_4 environments \mathcal{X}^+ and \mathcal{X}^- . The manifolds are parameterised by q (that moves along the degenerate set, represented by a black line) and s (that breaks the degeneracy). (b) Energy (top) and ^{13}C chemical shieldings (bottom) of a CH_4 molecule that follows the manifolds in panel (a); the zero of the two quantities is set to the values for the ideal tetrahedral geometry. (c) PCA projection of the manifolds computed in the bispectrum $|\mathcal{X}^{(3)}\rangle$ space. (d) Correlation plot of the distances between two points k and k' along both manifolds, computed based on the power spectrum ($d_{kk'}^{(2)}$) or the bispectrum ($d_{kk'}^{(3)}$).

the ^{13}C NMR chemical shift, and extensive properties such as molecular energy, are very different as they depend substantially on 4-body correlations.

A Gaussian process regression model based on a non-linear kernel built on the SOAP power spectrum (equivalent to the 3-body correlation, $|\mathcal{X}^{(2)}\rangle$, see SI) gives very large errors not just along the $s = 0$ line of degeneracy, but also for structures that are not exactly indistinguishable according to the power spectrum (top panels in Fig. 3). This underscores the fact that the existence of manifolds of degenerate structures introduces a distortion of the feature space (Fig. 1c), and hinders the ability to perform regression regardless of whether strictly degenerate pairs are included in the training. Because

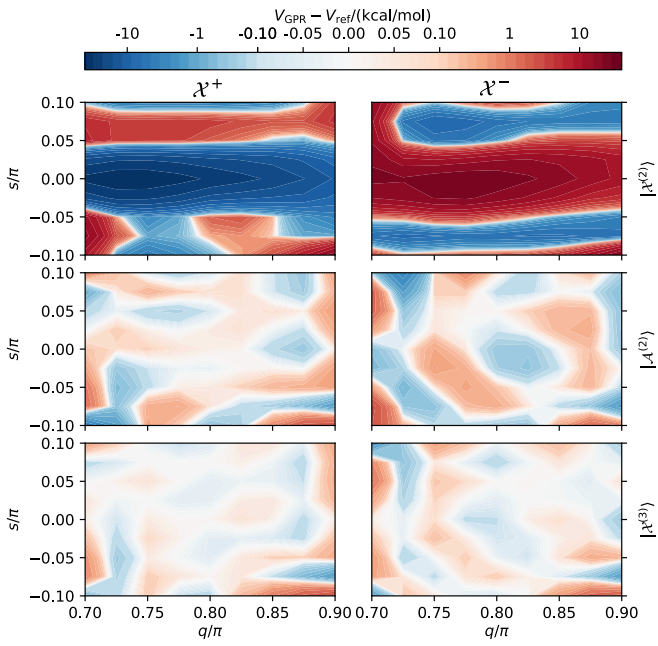


FIG. 3. Error in the prediction of the molecular energy for CH_4 configurations along the manifold depicted in Fig. 2c and d, using a GPR model based on a non-linear kernel built on the C-centred SOAP power spectrum (top), the C-centred bispectrum (bottom) and a combination of C and H-centred power spectra (middle).

they are ultimately based on the same unordered sets of triangles, Behler-Parrinello “atom-centered symmetry functions” [1], the FCHL descriptors of von Lilienfeld and coworkers [22], the MBTR descriptor of Rupp [23], and the smooth version of the DeepMD framework [24] will also suffer from the same problem.

The observation that a large manifold of CH_4 structures is un-learnable using 2- and 3-body descriptors paints a gloomy picture of the possibility of building a statistical learning framework based on such invariants, and is at odds with the empirical success of machine-learned potentials for molecules and condensed phases. One way to lift the degeneracy is to also consider features centred on the H atoms. Indistinguishability of atom-configuration pairs resulting from the construction in Fig. 1b is broken by centring somewhere outside the bisecting A plane, because the distance from the centre to $[+]$ and $[-]$ is then different. Every structure of this kind contains at least one atom outside the bisecting plane, so there is always an atom that can be centred on to resolve the degeneracy. Indeed, a model that combines C and H-centred non-linear kernels can approximate the molecular energy to reasonable (and improvable) accuracy, including configurations along the degenerate manifold (see Fig. 3, middle panels).

It is also possible to use higher body-order features to differentiate between \mathcal{X}^+ and \mathcal{X}^- . This can be done

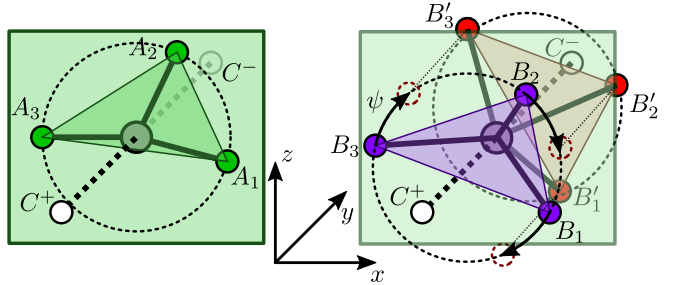


FIG. 4. (left) Construction of a pair of environments that are chiral mirror images but have the same chiral $|\mathcal{X}^{(3)}\rangle$ features. The A points lie in the xz plane, along a circle centred on the origin. C^\pm points lie along the y axis, symmetric about the origin. (right) a pair of inequivalent structures with the same chiral $|\mathcal{X}^{(3)}\rangle$ features. The B and B' points lie on circles centred on the origin, and then shifted by the same amount above and below the xz plane. One of the sets of points is then twisted by an angle ψ around y .

using e.g. the 4-body correlation, $|\mathcal{X}^{(3)}\rangle$, which corresponds to the unordered list of tetrahedra formed by the central atom and three of its neighbors and is equivalent to the bispectrum. Fig. 2c shows that the degeneracy in feature space is lifted by the bispectrum, while Fig. 2d shows that the presence of a degeneracy is apparent by comparing environment distances computed based on $|\mathcal{X}^{(2)}\rangle$ and $|\mathcal{X}^{(3)}\rangle$ (which we indicate with $d^{(2)}$ and $d^{(3)}$), as one recognizes pairs of environments that are very close together in power spectrum coordinates, but well separated by the bispectrum. The bottom panels of Fig. 3 show that the resolving power of the bispectrum results in an energy model with an error that is roughly half of that obtained by a multi-center, power-spectrum-based model. However, the bispectrum is not a unique descriptor either. While it does differentiate between the tetrahedral CH_4 environments, one can build pairs of environments that have the same 4-body correlations without being superimposable by proper (Fig. 4a) or improper (Fig. 4b) rotations. Note that the environments in Fig. 4a are chiral (mirror) images of each other, but the bispectrum does not distinguish them because the tetrahedra it is composed of are *not* chiral. [25] Approaches such as the moment tensor potentials [18] and the atomic cluster expansion [17] allow in principle – but at high cost – to further resolve degeneracies by including arbitrary body-orders of correlation.

To assess the relevance of these considerations for more complex modelling problems, let us now consider the database of silicon structures from Ref. 26. We start by computing an expansion of $|\mathcal{X}^{(2)}\rangle$ and $|\mathcal{X}^{(3)}\rangle$ on a basis of radial functions and spherical harmonics. We also compute the distance $d_{ii'}^{(v)}$ between the environments centered on atoms i, i' , as the Euclidean distance between the corresponding feature vectors. To reduce the impact of the much larger dimensionality of $|\mathcal{X}^{(3)}\rangle$, we select

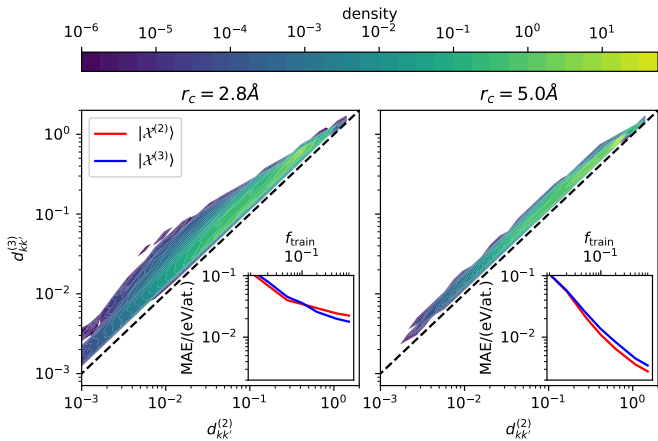


FIG. 5. An analysis of atom-centered representations of a database of Si structures. The main panels show the joint distribution of environment distances, $d_{kk'}^{(2)}$ and $d_{kk'}^{(3)}$, computed respectively from $|\mathcal{X}^{(2)}\rangle$ and $|\mathcal{X}^{(3)}\rangle$. Insets show learning curves for a model predicting the energy of the structures, built using 3 and 4-body representations and a Gaussian kernel. Left panels are based on a cutoff of 2.8 Å, right panels are based on a cutoff of 5.0 Å.

using CUR [27, 28] the 300 most significant components. The left panel in Figure 5 shows clear signals of the vicinity to a degenerate manifold, when using a short-range cutoff that only encompasses the nearest-neighbors shell. Indeed, pairs of environments can be found for which $d_{ii'}^{(3)}$ is almost 30 times larger than $d_{ii'}^{(2)}$, similar to what we observed in the artificial CH₄ dataset (Fig. 2d). We propose that the joint distance distributions can be used as a diagnostic tool to identify the presence of (near)-degenerate pairs of structures in a dataset. The right panel shows the same figure for a longer cutoff. Here, the resolving power of $|\mathcal{X}^{(2)}\rangle$ is comparable to that of the higher-order representation, with $d^{(2)}$ being at most a factor of 2 smaller than $d^{(3)}$. This suggests that degenerate structures become “less dense” as the number of neighbors is increased, which is consistent with the empirical observation that adding points to the construction in Fig. 1 increases the codimension of this particular set of indistinguishable configurations. At present, we cannot rigorously prove or disprove a more general statement. These observations are reflected in the performance of a ML model for the cohesive energy of Si configurations. In the case of the short-range cutoff, the model based on $|\mathcal{X}^{(3)}\rangle$ marginally outperforms that based on $|\mathcal{X}^{(2)}\rangle$, while the opposite is true for the 5.0 Å cutoff model. The differences are small, and sensitive to the details of the model. This suggests that when learning an atom-centred decomposition of an extensive property, such as the energy, at least to the relatively crude accuracy level of this example, the performance is minimally affected by the presence of near-degenerate structures. A low-body-order model may even outperform its higher-

order counterpart, e.g., due to the linear link to 2 and 3-body potentials that provide the leading-order contribution to the energy. However, it is clear that, in addition to long-range interactions [29], the presence of degeneracies that we have discovered also will limit the ultimate accuracy that can be achieved.

Overall, the results we have shown indicate that despite the remarkable success of ML models that describe atomic structures in terms of n -body correlations features, there is still work to do to understand fully how the configuration space of a set of atoms is mapped onto symmetry-adapted representations. The problem is to construct a representation which is (i) injective; (ii) smooth with smooth inverse; (iii) and invariant under isometries and permutations. An obvious, but ineffective, solution is to use the union of *all* n -point correlations [17, 18]. Pragmatically, one can proceed as we do here for the silicon dataset, increasing the correlation order until all configurations in a given training set are distinguishable, followed by a sparsification procedure along the lines of [28]. It is, however, desirable to know *a priori* which features are required to guarantee (i–iii). For example, we may ask whether there is a fixed finite \bar{n} such that all higher-order n -points correlations can be recovered from the \bar{n} -point correlation. There are at least two perspectives from which to pursue questions of this kind: signal processing and invariant theory.

In the signal processing (phase retrieval) literature it has long been known that the power spectrum (3-point correlations) is insufficient to reconstruct *most* signals, while the bi-spectrum uniquely identifies translation-invariant and compact signals [30–32]. On the other hand, Ref. [30] provides a range of elementary examples establishing that no correlation order suffices to reconstruct all periodic signals. Nevertheless, stable bispectrum inversion has been shown to work well in practice due to the fact the *most* signals can be reconstructed from it; see e.g. [33, 34] and references therein. These results have a striking parallel to the our own observations regarding the reconstruction of an atomic environment and in particular suggest that *in theory* no \bar{n} -point correlation may suffice to reconstruct the environment.

Still, since atomic environments can be thought of as a very restrictive class of signals, the invariant theory perspective may shed additional light on our questions. The perspective of Boutin and Kemper [21] appears to be particularly useful, establishing conditions under which a points cloud can be reconstructed from the histogram of distances. The problem we tackle here is closely related: degeneracy of two centred environments with respect to n -body correlations implies degeneracy of the point clouds consisting of the neighbors with respect to $n - 1$ body correlations. For example, Fig. 1a, implies that the length-histogram of the neighbours lying on the circle are degenerate (indeed, this is the example given in Fig. 4 in Ref.[21]). Similarly, Fig 4, which shows *environ-*

ments that are degenerate with respect to the 4-body correlation (tetrahedron histograms) is also degenerate with respect to the 3-body correlations (triangle histograms) of the *entire* structure. A similar approach may therefore help determine tight bounds on the codimension of the degenerate manifold. As far as we are aware, however, there are no rigorous results in this direction.

While the problem of formulating an injective feature map is of fundamental importance – particularly when considering the use for generative models that require inverting the relation between a representation and the underlying structure – the results we present here suggest that low-correlation order representations may suffice in practice, especially when high accuracy is not required. In particular, the presence of many neighbors or of different species (that provide distinct “labels” to associate groups of distances and angles to specific atoms), and the possibility of using representations centred on nearby atoms to lift the degeneracy of environments reduces the detrimental effects of the lack of uniqueness of the power spectrum, when learning extensive properties such as the energy. This explains, retrospectively, the considerable success of ML models based on non-injective representations. However, introducing higher order invariants that lift the degeneracies may enable better choices of model parameters. Diagnostic tools such as the joint distance histogram that we introduce here can help identify problematic parts of datasets, and give more confidence on the reliability of simple-to-compute low-order invariant representations.

MJW, SP and MC acknowledge funding by the Swiss National Science Foundation (Project No. 200021-182057). CO acknowledges funding by the Leverhulme trust, RPG-2017-191.

C. Corminboeuf, and M. Ceriotti, *ACS Cent. Sci.* **5**, 57 (2019).

- [10] D. M. Wilkins, A. Grisafi, Y. Yang, K. U. Lao, R. A. DiStasio, and M. Ceriotti, *Proc. Natl. Acad. Sci. U. S. A.* **116**, 3401 (2019).
- [11] A. Glielmo, P. Sollich, and A. De Vita, *Phys. Rev. B* **95**, 214302 (2017).
- [12] A. Grisafi, D. M. Wilkins, G. Csányi, and M. Ceriotti, *Phys. Rev. Lett.* **120**, 036002 (2018).
- [13] A. P. Bartók, R. Kondor, and G. Csányi, *Phys. Rev. B* **87**, 184115 (2013).
- [14] S. Chmiela, A. Tkatchenko, H. E. Sauceda, I. Poltavsky, K. T. Schütt, and K.-R. Müller, *Sci. Adv.* **3**, e1603015 (2017), arXiv:1611.04678.
- [15] O. A. von Lilienfeld, *Angew. Chem. Int. Ed.* **57**, 4164 (2018).
- [16] M. J. Willatt, F. Musil, and M. Ceriotti, *J. Chem. Phys.* **150**, 154110 (2019).
- [17] R. Drautz, *Phys. Rev. B* **99**, 014104 (2019).
- [18] A. Shapeev, *Multiscale Model. Simul.* **14**, 1153 (2016).
- [19] C. van der Oord, G. Dusson, G. Csanyi, and C. Ortner, (2019), arXiv:1910.06010.
- [20] A. P. Thompson, L. P. Swiler, C. R. Trott, S. M. Foiles, and G. J. Tucker, *J. Comput. Phys.* **285**, 316 (2015).
- [21] M. Boutin and G. Kemper, *Adv. Appl. Math.* **32**, 709 (2004).
- [22] F. A. Faber, A. S. Christensen, B. Huang, and O. A. Von Lilienfeld, *J. Chem. Phys.* **148**, 241717 (2018).
- [23] H. Huo and M. Rupp, (2017), arXiv:1704.06439.
- [24] L. Zhang, J. Han, H. Wang, W. Saidi, R. Car, and W. E, in *Advances in Neural Information Processing Systems 31*, edited by S. Bengio, H. Wallach, H. Larochelle, K. Grauman, N. Cesa-Bianchi, and R. Garnett (Curran Associates, Inc., 2018) pp. 4436–4446.
- [25] All body-order correlations above $\nu = 3$, when defined as an average over proper rotations, are sensitive to chirality and can differentiate between enantiomers. When learning non-chiral properties, such as the energy, one can average over inversion. Unless otherwise specified, in this work $|\mathcal{X}^{(3)}\rangle$ indicates the non-chiral version.
- [26] A. P. Bartók, J. Kermode, N. Bernstein, and G. Csányi, *Phys. Rev. X* **8**, 041048 (2018), arXiv:1805.01568.
- [27] M. W. Mahoney and P. Drineas, *Proc. Natl. Acad. Sci. U. S. A.* **106**, 697 (2009).
- [28] G. Imbalzano, A. Anelli, D. Giofré, S. Klees, J. Behler, and M. Ceriotti, *J. Chem. Phys.* **148**, 241730 (2018).
- [29] A. Grisafi and M. Ceriotti, *J. Chem. Phys.* **151**, 204105 (2019).
- [30] J. I. Yellott and G. J. Iverson, *J. Opt. Soc. Am. A, JOSAA* **9**, 388 (1992).
- [31] R. Kondor, , 1 (2018), arXiv:1803.01588.
- [32] R. Kakarala, *J. Math. Imaging Vis.* **44**, 341 (2012), arXiv:0902.0196.
- [33] T. Bendory, N. Boumal, C. Ma, Z. Zhao, and A. Singer, *IEEE Trans. Signal Process.* **66**, 1037 (2018).
- [34] A. S. Bandeira, B. Blum-Smith, J. Kileel, A. Perry, J. Weed, and A. S. Wein, (2017), arXiv:1712.10163 [math.ST].

* These two authors contributed equally

† c.ortner@warwick.ac.uk

‡ g121@cam.ac.uk

§ michele.ceriotti@epfl.ch

- [1] J. Behler and M. Parrinello, *Phys. Rev. Lett.* **98**, 146401 (2007).
- [2] W. J. Szlachta, A. P. Bartók, and G. Csányi, *Phys. Rev. B* **90**, 104108 (2014).
- [3] A. P. Bartók, M. C. Payne, R. Kondor, and G. Csányi, *Phys. Rev. Lett.* **104**, 136403 (2010).
- [4] R. Kobayashi, D. Giofré, T. Junge, M. Ceriotti, and W. A. Curtin, *Phys. Rev. Mater.* **1**, 053604 (2017).
- [5] N. Lubbers, J. S. Smith, and K. Barros, *J. Chem. Phys.* **148**, 241715 (2018).
- [6] M. Gastegger, J. Behler, and P. Marquetand, *Chem. Sci.* **8**, 6924 (2017).
- [7] A. Glielmo, C. Zeni, and A. De Vita, *Phys. Rev. B* **97**, 184307 (2018).
- [8] K. T. Schütt, F. Arbabzadah, S. Chmiela, K. R. Müller, and A. Tkatchenko, *Nat. Commun.* **8**, 13890 (2017).
- [9] A. Grisafi, A. Fabrizio, B. Meyer, D. M. Wilkins,

On the Completeness of Atomic Structure Representations

Supplementary material

1 Power spectrum

1.1 Moving points

Take two points \mathbf{r}_+ and \mathbf{r}_- which share the same distance to the origin, $r_+ = r_-$, and are not parallel or antiparallel. It will prove useful to construct a complete orthonormal basis from the two points as follows,

$$\hat{\mathbf{i}} = \frac{\mathbf{r}_+ + \mathbf{r}_-}{|\mathbf{r}_+ + \mathbf{r}_-|} \quad (1)$$

$$\hat{\mathbf{j}} = \frac{\mathbf{r}_+ - \mathbf{r}_-}{|\mathbf{r}_+ - \mathbf{r}_-|} \quad (2)$$

$$\hat{\mathbf{k}} = \frac{\mathbf{r}_+ \times \mathbf{r}_-}{|\mathbf{r}_+ \times \mathbf{r}_-|}. \quad (3)$$

Note that $\hat{\mathbf{i}}$ and $\hat{\mathbf{j}}$ are orthogonal because $r_+ = r_-$.

Our goal is to introduce more points in such a way that all distance-angle triplets formed by pairs of points and the origin are the same in two configurations (+) and (-), formed by removing either \mathbf{r}_- or \mathbf{r}_+ . This will ensure the origin-centred power spectra of (+) and (-) are equal too. Any point we add falls into one of two classes.

1.2 Points in the bisecting plane

The bisecting plane is spanned by $\hat{\mathbf{i}}$ and $\hat{\mathbf{k}}$. Any point with no component along $\hat{\mathbf{j}}$ lies in this plane and makes the same angle with \mathbf{r}_+ and \mathbf{r}_- . Adding points in this plane contributes exactly the same distance-angle triplets to (+) and (-) and does not break indistinguishability. But if one only adds points in this way, the bisecting plane is a plane of symmetry before \mathbf{r}_+ or \mathbf{r}_- is removed, and (+) and (-) are therefore mirror images of each other. We must therefore add at least one point outside the bisecting plane.

1.3 Points outside the bisecting plane

Any point outside the bisecting plane has a non-zero $\hat{\mathbf{j}}$ component,

$$\mathbf{r} = a\hat{\mathbf{i}} + b\hat{\mathbf{j}} + c\hat{\mathbf{k}}. \quad (4)$$

Such a point makes different angles, θ_+ and θ_- , with \mathbf{r}_+ and \mathbf{r}_- and contributes different distance-angle triplets to (+) and (-), breaking indistinguishability. To recover indistinguishability, we must therefore add another point outside the bisecting plane,

$$\mathbf{r}' = d\hat{\mathbf{i}} + e\hat{\mathbf{j}} + f\hat{\mathbf{k}}. \quad (5)$$

If $r \neq r'$ indistinguishability is not recovered, so we must have

$$a^2 + b^2 + c^2 = d^2 + e^2 + f^2. \quad (6)$$

Since only (+) includes θ_+ and only (−) includes θ_- , the only way to recover indistinguishability is by introducing θ_- into (+) and θ_+ into (−) with the new point \mathbf{r}' . This in combination with Eq. (6) and $r_+ = r_-$ is equivalent to the following constraints,

$$\mathbf{r} \cdot \mathbf{r}_+ = \mathbf{r}' \cdot \mathbf{r}_- \quad (7)$$

$$\mathbf{r} \cdot \mathbf{r}_- = \mathbf{r}' \cdot \mathbf{r}_+. \quad (8)$$

The sum and difference of these equations gives

$$\mathbf{r} \cdot \hat{\mathbf{i}} = \mathbf{r}' \cdot \hat{\mathbf{i}} \quad (9)$$

$$\mathbf{r} \cdot \hat{\mathbf{j}} = -\mathbf{r}' \cdot \hat{\mathbf{j}}, \quad (10)$$

which fixes \mathbf{r}' to be

$$\mathbf{r}' = a\hat{\mathbf{i}} - b\hat{\mathbf{j}} + f\hat{\mathbf{k}}. \quad (11)$$

The length constraint Eq. (6) fixes the remaining component up to its sign,

$$\mathbf{r}' = a\hat{\mathbf{i}} - b\hat{\mathbf{j}} \pm c\hat{\mathbf{k}}. \quad (12)$$

We choose the solution with the minus sign because otherwise \mathbf{r} and \mathbf{r}' are reflections of each other through the bisecting plane and (+) and (−) are mirror images, which is precisely what set out to avoid.

1.4 In combination

By adding points in the two ways just described, one constructs (+) and (−) configurations that are indistinguishable through their origin-centred power spectra. Since there must be at least one point outside the bisecting plane to avoid mirror images, and such points can only be present in pairs, the simplest (+) and (−) configurations comprise four points excluding the centre: one point in the bisecting plane, two outside it and \mathbf{r}_+ or \mathbf{r}_- .

A transparent parameterisation is obtained by aligning $\hat{\mathbf{i}}$, $\hat{\mathbf{j}}$ and $\hat{\mathbf{k}}$ with the x , y and z axes. The four-particle case is depicted in Fig. 1 of the main text, with $\hat{\mathbf{i}}$ aligned along the z axis, $\hat{\mathbf{j}}$ along the y axis and $\hat{\mathbf{k}}$ along the x axis,

$$\mathbf{r}_+ = a\hat{\mathbf{y}} + b\hat{\mathbf{z}} \quad (13)$$

$$\mathbf{r}_- = -a\hat{\mathbf{y}} + b\hat{\mathbf{z}} \quad (14)$$

$$\mathbf{r}_1 = c\hat{\mathbf{x}} + d\hat{\mathbf{z}} \quad (15)$$

$$\mathbf{r}_2 = e\hat{\mathbf{x}} + f\hat{\mathbf{y}} + g\hat{\mathbf{z}} \quad (16)$$

$$\mathbf{r}_3 = -e\hat{\mathbf{x}} - f\hat{\mathbf{y}} + g\hat{\mathbf{z}}. \quad (17)$$

There are seven free parameters, a, b, c, d, e, f, g , leaving a codimension of two. Adding an extra point in the bisecting plane increases the codimension by one, and adding an extra pair of points outside the bisecting plane increases the codimension by three. In spherical polar coordinates we have

$$\mathbf{r}_+ = r [\cos(q)\hat{\mathbf{y}} + \sin(q)\hat{\mathbf{z}}] \quad (18)$$

$$\mathbf{r}_- = r [-\cos(q)\hat{\mathbf{y}} + \sin(q)\hat{\mathbf{z}}] \quad (19)$$

$$\mathbf{r}_1 = r' [\cos(\alpha)\hat{\mathbf{x}} + \sin(\alpha)\hat{\mathbf{z}}] \quad (20)$$

$$\mathbf{r}_2 = r'' [\sin(\theta) \cos(\phi)\hat{\mathbf{x}} + \sin(\theta) \sin(\phi)\hat{\mathbf{y}} + \cos(\theta)\hat{\mathbf{z}}] \quad (21)$$

$$\mathbf{r}_3 = r'' [-\sin(\theta) \cos(\phi)\hat{\mathbf{x}} - \sin(\theta) \sin(\phi)\hat{\mathbf{y}} + \cos(\theta)\hat{\mathbf{z}}], \quad (22)$$

which is a special case of

$$\mathbf{r}_+ = r [-\sin(s)\hat{\mathbf{x}} + \cos(s) \cos(q)\hat{\mathbf{y}} + \cos(s) \sin(q)\hat{\mathbf{z}}] \quad (23)$$

$$\mathbf{r}_- = r [-\sin(s)\hat{\mathbf{x}} - \cos(s) \cos(q)\hat{\mathbf{y}} + \cos(s) \sin(q)\hat{\mathbf{z}}]. \quad (24)$$

Any variation of s away from $s = 0$ breaks the indistinguishability of (+) and (−). The variation of q and s with every other parameter fixed is used to explore the (+) and (−) property surfaces in the main text (Fig. 2 onwards).

1.5 Moving the centre

For any point \mathbf{r} outside the bisecting plane we have

$$|\mathbf{r}_+ - \mathbf{r}| \neq |\mathbf{r}_- - \mathbf{r}|, \quad (25)$$

because $r_+ = r_-$. By centring on the point \mathbf{r} indistinguishability of the atom configurations is broken since the distance-angle triplet $(|\mathbf{r}_+ - \mathbf{r}|, |\mathbf{r}_+ - \mathbf{r}|, 0)$ appears once more in (+) than in (−). As mentioned previously, there must be at least one atom outside the bisecting plane for the atom configurations (+) and (−) not to be mirror images of each other, so distinguishability of the atom configurations can always be recovered by centring the power spectrum on such an atom.

1.6 More moving points

Throughout the discussion above we supposed the configurations (+) and (−) differ only in the position of two points, \mathbf{r}_+ and \mathbf{r}_- . We added points to both (+) and (−) satisfying constraints involving only distances of points to the origin and dot products with unit vectors $\hat{\mathbf{i}}, \hat{\mathbf{j}}, \hat{\mathbf{k}}$ generated by \mathbf{r}_+ and \mathbf{r}_- .

Suppose instead we have multiple points like \mathbf{r}_+ which feature only in (+) and \mathbf{r}_- which feature only in (−). There must of course be the same number of points in (+) and (−) for the configurations to be indistinguishable, so we can group together the \mathbf{r}_+ and \mathbf{r}_- points into pairs. Suppose we choose these pairs in a special way, such each point in a pair is the same distance to the origin and every pair generates the same unit vectors through Eqs. (1-3). Then the k^{th} pair has the following form,

$$\mathbf{r}_+^k = q_k \hat{\mathbf{i}} + \Delta_k \hat{\mathbf{j}} \quad (26)$$

$$\mathbf{r}_-^k = q_k \hat{\mathbf{i}} - \Delta_k \hat{\mathbf{j}}. \quad (27)$$

Clearly,

$$\mathbf{r}_-^k \cdot \mathbf{r}_-^l = \mathbf{r}_+^k \cdot \mathbf{r}_+^l, \quad (28)$$

which shows that every distance-angle triplet in (+) involving the centre and two \mathbf{r}_+ points is the same as a distance-angle triplet in (−) involving the centre and two \mathbf{r}_- points. Furthermore, since $\hat{\mathbf{i}}, \hat{\mathbf{j}}, \hat{\mathbf{k}}$ are common to all pairs, the constraints for adding the same points to (+) and (−) are identical to before. In other words, adding a point \mathbf{r}'_+ to (+) and \mathbf{r}'_- to (−) preserves indistinguishability of (+) and (−) if these points have the form of Eqs. (26-27). Adding such a pair increases the codimension by one.

1.7 High-multiplicity degeneracies

The construction discussed in the previous sections generates pairs of structures with the same power spectrum. It is also possible, however, to construct sets of more than two degenerate structures. An

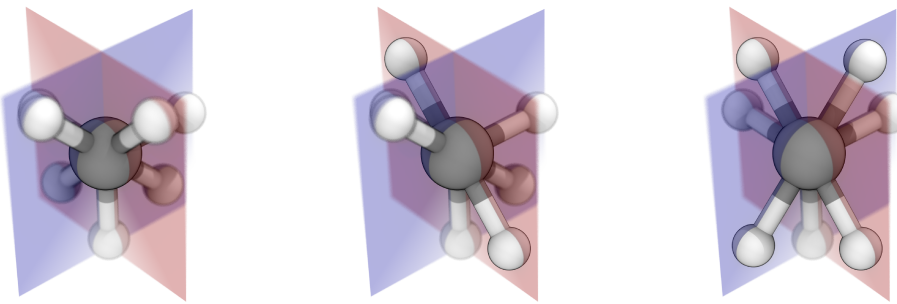


Figure S1: Three different structures with the same three-body representation

example of a group of three distinct structure having the same 3-body representation is shown in Fig. S1. The atomic coordinates associated with the three structures are:

$$\begin{pmatrix} \begin{bmatrix} \cos(0) \\ \sin(0) \\ 0 \end{bmatrix} \begin{bmatrix} \cos(-\frac{\pi}{4}) \\ \sin(-\frac{\pi}{4}) \\ 0 \end{bmatrix} \begin{bmatrix} \cos(-\frac{\pi}{2}) \\ \sin(-\frac{\pi}{2}) \\ 0 \end{bmatrix} \begin{bmatrix} \cos(\frac{3\pi}{4}) \\ \sin(\frac{3\pi}{4}) \\ 0 \end{bmatrix} \begin{bmatrix} 0 \\ \cos(\frac{-3\pi}{4}) \\ \sin(\frac{-3\pi}{4}) \end{bmatrix} \begin{bmatrix} 0 \\ \cos(-\frac{\pi}{2}) \\ \sin(-\frac{\pi}{2}) \end{bmatrix} \begin{bmatrix} 0 \\ \cos(\frac{\pi}{4}) \\ \sin(\frac{\pi}{4}) \end{bmatrix} \end{pmatrix}, \quad (29)$$

$$\begin{pmatrix} \begin{bmatrix} \cos(0) \\ \sin(0) \\ 0 \end{bmatrix} \begin{bmatrix} \cos(-\frac{\pi}{4}) \\ \sin(-\frac{\pi}{4}) \\ 0 \end{bmatrix} \begin{bmatrix} \cos(-\frac{\pi}{2}) \\ \sin(-\frac{\pi}{2}) \\ 0 \end{bmatrix} \begin{bmatrix} \cos(\frac{3\pi}{4}) \\ \sin(\frac{3\pi}{4}) \\ 0 \end{bmatrix} \begin{bmatrix} 0 \\ \cos(\frac{3\pi}{4}) \\ \sin(\frac{3\pi}{4}) \end{bmatrix} \begin{bmatrix} 0 \\ \cos(-\frac{\pi}{2}) \\ \sin(-\frac{\pi}{2}) \end{bmatrix} \begin{bmatrix} 0 \\ \cos(-\frac{\pi}{4}) \\ \sin(-\frac{\pi}{4}) \end{bmatrix} \end{pmatrix}, \quad (30)$$

$$\begin{pmatrix} \begin{bmatrix} \cos(0) \\ \sin(0) \\ 0 \end{bmatrix} \begin{bmatrix} \cos(\frac{\pi}{4}) \\ \sin(\frac{\pi}{4}) \\ 0 \end{bmatrix} \begin{bmatrix} \cos(-\frac{\pi}{2}) \\ \sin(-\frac{\pi}{2}) \\ 0 \end{bmatrix} \begin{bmatrix} \cos(-\frac{3\pi}{4}) \\ \sin(-\frac{3\pi}{4}) \\ 0 \end{bmatrix} \begin{bmatrix} 0 \\ \cos(\frac{3\pi}{4}) \\ \sin(\frac{3\pi}{4}) \end{bmatrix} \begin{bmatrix} 0 \\ \cos(-\frac{\pi}{2}) \\ \sin(-\frac{\pi}{2}) \end{bmatrix} \begin{bmatrix} 0 \\ \cos(-\frac{\pi}{4}) \\ \sin(-\frac{\pi}{4}) \end{bmatrix} \end{pmatrix}. \quad (31)$$

This example can be obtained by extending the counterexample discussed above, adding further points. Start from the planar example showed in Fig. 1a, and label the two degenerate configurations \mathcal{X}^+ and \mathcal{X}^- . These structures can be extended by adding an arbitrary number of points to both configurations, lying on a plane perpendicular to the plane of the figure, without lifting the degeneracy. Let's take structure \mathcal{X}^+ , and extend it with the same structure \mathcal{X}^+ in the perpendicular plane, forming a configuration \mathcal{X}^{++} . Similarly, one can obtain two additional structures \mathcal{X}^{--} and \mathcal{X}^{+-} . In all cases the set of distance-angle triplets consist of three groups. One that contains the neighbors from the initial structure, one that contains those from the additional atoms in the perpendicular plane, and a third one for which one neighbor comes from the initial structure and the other from the additional atoms. Since the structures \mathcal{X}^+ and \mathcal{X}^- are indistinguishable we automatically see that first two distance-angle groups coincide in all the three extended structures. One only needs to check whether the 3-body correlations between the two groups, which are determined by the mutual placement of the structures on the two orthogonal planes, are the same in the three structures. The relative orientation is in turn determined by a single angle. We could determine, by trial-and-error, a value of the mutual orientation that leads to the three structures being degenerate with each other.

2 Bispectrum

Fig. S2 shows how to generate pairs of atom configurations with the same origin-centred bispectrum. In the first three panels an atom sits at the origin O and at every polygon vertex A, B, C , etc. By adding another atom an arbitrary distance above $[+]$ or below $[-]$ the plane of the page, such that the lines $O[+]$ and $O[-]$ are orthogonal to the plane, one obtains two atom configurations $(+)$ and $(-)$ which share the same origin-centred bispectrum, even if they cannot be superimposed by proper rotations (they are chiral mirror images of each other).

In panel 1., the triangle ABC lies in the plane of the page. Every tetrahedron containing O and $[+]$ as vertices can be superimposed on another tetrahedron containing O and $[-]$ as vertices by a rigid rotation. However, if two of the angles a, b, c are different, the atom configurations are non-superimposable mirror images of each other. There are various free parameters: two of the angles, the circle radius, the distance separating $[+]$ and $[-]$ and even the number of atoms on the circle. This last freedom is demonstrated in panel 2. Panel 3. shows the simplest example we have found of two atom configurations which are not congruent – i.e. that cannot be superimposed by either proper or improper rotations – but share the same bispectrum. The congruent triangles ABC and DEF are parallel with the plane of the page and share the same distance to it. As with the other examples, every tetrahedron containing O and $[+]$ as vertices can be superimposed on another tetrahedron containing O and $[-]$ as vertices by a rigid rotation, but the atom configurations $(+)$ and $(-)$ are not congruent. The position of the points $[+]$ and $[-]$ are shown explicitly in panel 4, which corresponds to the same construction as panel 3 when viewed from the side. There are six free parameters: two of the angles in a, b, c , the torsion angle between the triangles, the distance between the triangles, the circle radius and the distance between $[+]$ and $[-]$. This example can also be generalised as in panel 2. with any asymmetric polygon instead of a triangle.

In all of the examples depicted in the figure, one can add more atoms along the axis containing O , $[+]$, $[-]$ to the atom configuration $(+)$, provided one also adds more atoms along the same axis to $(-)$, such that every atom along this axis in $(+)$ maps on to a corresponding atom in $(-)$ under a reflection through the plane of the page.

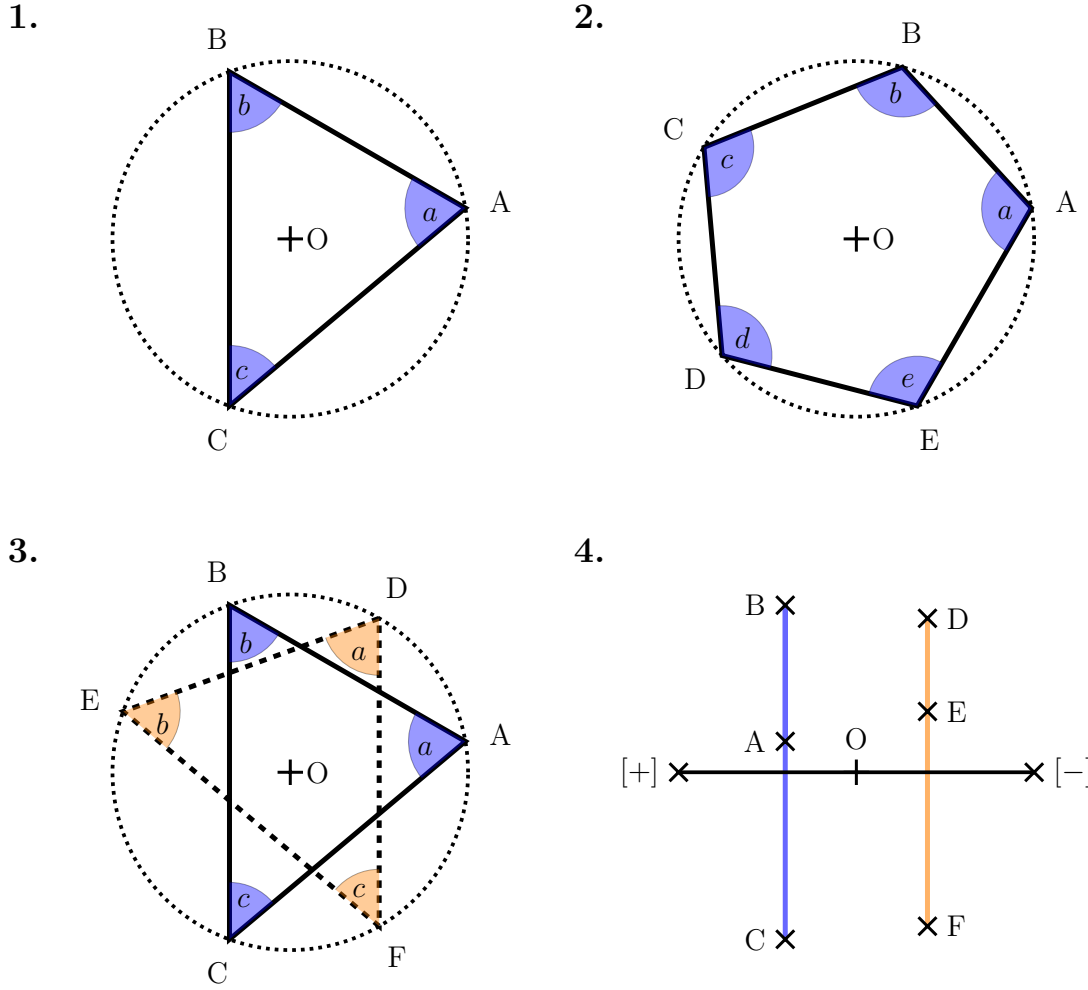


Figure S2: Four diagrams showing how to generate pairs of atom configurations with the same origin-centred bispectrum. In the first three panels an atom sits at the origin O and at every polygon vertex A , B , C , etc. By adding another atom an arbitrary distance above $[+]$ or below $[-]$ the plane of the page, such that the lines $O[+]$ and $O[-]$ are orthogonal to the plane, one obtains two atom configurations $(+)$ and $(-)$ which share the same origin-centred bispectrum. Panel 4 shows the construction in panel 3 from the side.

3 Regression models

In order to verify how the discussed degeneracies influence the performance of machine learning potentials, we used Kernel Ridge Regression (KRR). The following atomic kernel was used,

$$k_{ij} = \exp \left(-(2 - 2 \sum_q f_{iq} f_{jq}) / \sigma_k^2 \right), \quad (32)$$

where f_{iq} and f_{jq} are features (power spectrum or bispectrum) describing the environment of atoms i and j respectively. We used atom-centred Gaussians with a width of 0.5\AA to construct the atomic density. Since all atoms are at the same distance from the centre, we set a cutoff of 2\AA and computed SOAP features with $n_{\max} = 1$ Gaussian type orbital radial basis function, and $l_{\max} = 4$ angular channels. In the case of the C-centered models (top and middle panels of Fig. 3) this kernel was applied directly, while in the case of the C and H-centered models (bottom panel of Fig. 3) we used the standard modification

$$K_{IJ} = \sum_{ij} k_{ij}, \quad (33)$$

where the K_{IJ} is the kernel between structures I and J , the summation runs over all atoms in structures I and J , and k_{ij} is the atomic kernel in Eq. (32). The exponential kernel parameter σ_k^2 and the L^2 regularization parameter were optimized by cross-validation for every learning setup. The predictions plotted in Fig. 3 are obtained by 2-fold cross-validation, and averaged over 100 random shuffles of the dataset.

In the case of silicon we used $n_{\max} = 8$ radial basis functions and $l_{\max} = 6$ spherical harmonics channels. This led to an enormous number of bispectrum components. To avoid artefacts from the huge difference in dimensionality between the 3 and 4-body representations, we applied CUR feature selection to filter out 300 features from the powerspectrum and likewise for the bispectrum. We used the kernel introduced earlier in KRR with $\sigma_k^2 = 0.02$ for the short range model ($r_c = 2.8\text{\AA}$) and $\sigma_k^2 = 0.2$ for the long range model ($r_c = 5.0\text{\AA}$). The L^2 regularization parameter was chosen independently for every training setup using cross-validation.

4 Dimensionality of the degenerate set

We briefly summarize our theoretical findings on the co-dimension of the degenerate set for the 3-body descriptor.

First, it is immediate that for one or two neighbours the histogram of triangles determines the neighbourhood up to symmetries. For three neighbours the same statement is still true, and follows from the fact that a tetrahedron is uniquely defined by the three faces which are given by the three $1 \leq i < j \leq 3$ elements of the histogram of triangles.

For four neighbours we have constructed a co-dimension 2 manifold of degenerate neighbourhood configurations. We now proceed to prove that this co-dimensionality is sharp: Given the histogram of triangles $\{(r_{ij}, r_{ij'}, \omega_{ijj'})\}$ we can define two polynomials

$$p_r = \prod_{j < j'} (r_j^2 - r_{j'}^2), \quad p_n = p_D(\{\mathbf{r}_{ij}\}) \prod_{kk'' \neq jj'} (r_{kk'}^2 - r_{jj'}^2)$$

where p_D is a polynomial defined in [1] with the following property (Theorem 2.6 in [1]): If $p_D(\{\mathbf{r}_j\}) \neq 0$ then the configuration $\{\mathbf{r}_j\}$ can be reconstructed from the histogram of distances $\{r_{jj'}\}$.

We now claim that, if either p_r or p_D is non-zero then the neighbourhood $\{\mathbf{r}_{ij}\}$ can be reconstructed up to symmetries. If p_r is non-zero then all distances r_{ij} are distinct hence the Gram matrix can be reconstructed and therefore also the neighbourhood (see the main text for more details).

If $p_r = 0$ but $p_n \neq 0$ (and hence $p_D \neq 0$) then according to [1, Thm. 2.6] we can reconstruct the positions of the neighbours \mathbf{r}_{ij} up to an isometry and permutation which is a free symmetry, and up to an unknown *translation* which we now need to reconstruct. To this end we note that the added condition $r_{kk'} \neq r_{jj'}$ in the definition of p_n means that the edges are all labelled. From these labels we can then get the labels for the corners. The issue that remains is that we still need to attach distances to the

corners: If all r_{ij} are distinct, then there is nothing to prove. If, say $r_{i1} = r_{i2}$ then this means we can identify these two lengths from the triangle $(r_{i1}, r_{i2}, \omega_{i12})$. But knowing r_{i1} we can identify r_{ij} from $(r_{i1}, r_{ij}, \omega_{i1j})$. Therefore we now know all distances r_{ij} to the corners \mathbf{r}_{ij} .

We can now return to determining the centre. If we have four or more neighbours that do not lie in a plane, then there is one possible centre. If all points lie in a plane then there are two possible centres but they are equivalent up to a reflection. If all points lie on a line then there is a circle of possible centres which are all equivalent up to rotations.

Thus, we have shown that for four or more neighbours, the set of degenerate neighbourhood structures are contained in an algebraic manifold which has at least co-dimension two.

References

- [1] Mireille Boutin and Gregor Kemper. On reconstructing n-point configurations from the distribution of distances or areas. *Adv. Appl. Math.*, 32(4):709–735, may 2004.